Unitary limit and its far-reaching impact on neutron matter

Francesca Sammarruca*
Department of Physics, University of Idaho, Moscow, Idaho 83844-0903, USA

(Received 23 August 2023; accepted 27 September 2023; published 13 October 2023)

This paper explores low-density neutron matter and its behavior in proximity to the unitary limit. To that end, unitary nucleon-nucleon potentials, with infinite $^1S_0$ neutron-neutron scattering lengths, are constructed and the Berstch parameter is discussed in relation to results from ultracold atomic gases. A focal point is unitarity as a constraint for neutron matter and the symmetry energy, a topic that has been discussed in the literature. I revisit some of those arguments and emphasize the relevance of keeping a firm link with low-energy nuclear physics for robust predictions of neutron-rich systems. The predictions are obtained from realistic few-nucleon forces based on chiral effective field theory at N^{3}LO.

DOI: 10.1103/PhysRevC.108.044310

I. INTRODUCTION

The physics of neutron matter (NM) spans a broad range of densities. At low density, it approaches universal behavior as a consequence of the large neutron-neutron scattering length in the spin-singlet channel. Around normal nuclear density, it is an appropriate laboratory to study neutron-rich nuclei, and, at even higher densities, it strongly constrains the physics of neutron stars. Although an idealized system, neutron matter also provides unique opportunities to test nuclear forces, because all low-energy constants appearing in the three-neutron forces are predicted at the two-neutron level.

The latest results from my group for the equation of state (EoS) of NM and the properties of the symmetry energy are based on high-quality nuclear forces constructed within the framework of chiral effective field theory (EFT) [1,2]. For the past several years, chiral EFT has been generally recognized as the most fundamental approach for developing nuclear interactions: it provides a systematic way to construct nuclear two- and many-body forces on an equal footing [3] and allows to assess theoretical uncertainties through an expansion controlled by an organizational scheme known as "power counting" [3]. Furthermore, chiral EFT maintains consistency with the underlying fundamental theory of strong interactions, quantum chromodynamics (QCD), through the symmetries and symmetry breaking mechanisms of low-energy QCD.

This work is a specific investigation of dilute NM within the same framework. Predictions are based on the EoS from Refs. [1,2], which are derived from two- and three-nucleon chiral forces consistently at N^{3}LO.

A strong motivation for studying the physics of low-density NM is its impact on the inner crust of neutron stars, where the nucleon density varies approximately from 10^{-3} to 0.08 fm^{-3}. In that region, matter consists of a mixture of very neutron-rich nuclei (arranged in a Coulomb lattice), electrons, and a superfluid neutron gas.

At low densities, the neutron-neutron interaction is dominated by the attractive component of the $^1S_0$ partial wave, which, although insufficient to bind two neutrons, leads to a virtual dineutron state and thus the large neutron-neutron scattering length in this channel, $a_s = -18.9(4)$ fm [4]. Therefore, even if the average distance between two neutrons is much larger than the effective range in the $^1S_0$ neutron-neutron interaction, $r_e = 2.75(11)$ fm [5], NM is still a strongly correlated system. Note that k_F^{-1}, being proportional to the cubic root of the unit volume, can be taken as an approximate measure of the average distance between fermions.

A unitary Fermi gas is an idealized system of fermions with a zero-range interaction having an infinite (negative) scattering length. All properties of this interacting gas are simply proportional to the corresponding ones in the noninteracting system at the same density. The model of a dilute quantum gas can describe diverse systems and can be applied in different areas of physics. At the low temperatures required to observe quantum phenomena in a dilute gas, the type of fermions and the exact form of the interaction become unimportant for the macroscopic properties of the system. For these reasons, results from the field of cold gases can give insight into systems such as NM at subnuclear densities. This unique feature of interacting Fermi gases—unitarity—can be generalized to any system of fermions subjected to mutual interactions with diverging scattering lengths. The unitary limit was first introduced in 1999 by Bertsch [6], who proposed to model low-density neutron matter as a Fermi gas where

$$r_e \ll k_F^{-1} \ll |a_s|, \quad \text{implying} \quad k_F|a_s| \gg 1. \tag{1}$$

Universality of unitary systems implies that the ground state energy at the unitary limit should be given by

$$E(k_F) = \xi E_{FG}(k_F), \tag{2}$$

where ξ is known as the Bertsch parameter and $E_{FG}(k_F)$ is the energy of the corresponding noninteracting Fermi gas.

*fsammarr@uidaho.edu

Measurements of the Berstch parameter with ultracold atomic gases reported values ranging from ≈0.36 to ≈0.51 [7–12].

In the physics of cold atoms near the Feshbach resonance [13], external magnetic fields allow the scattering length to be tuned arbitrarily. As mentioned above, in the regime of divergent scattering lengths, the gas is both dilute (the range of the interatomic potential is much smaller than the interparticle distance) and, at the same time, strongly interacting (the scattering length is much larger than the interparticle distance). Thus, the only scale in the unitary gas (at zero temperature) is the Fermi momentum of the system—hence, the universal rescaling of bulk observables.

Unitary Fermi gases have been obtained in the laboratory with ultracold trapped alkali atoms, where the effective range of the interaction is approximately equal to $10^{-4}k_F^{-1}$. In these experiments, it is possible to tune the interatom interaction from a weak to a strong coupling regime, and thus to explore the crossover from Bardeen-Cooper-Schrieffer (BCS) pairing with weakly attractive ($a_s < 0$) Cooper pairs to the Bose-Einstein condensation (BEC) of bound dimers ($a_s > 0$) [14–16]. Theoretical predictions for ξ range from 0.3 to 0.7 [6,17–24]. Variational Monte Carlo [25], Green's function Monte Carlo [26], and Brueckner-Hartree-Fock (BHF) [27] calculations of the EoS of low-density NM tend to cluster around $\xi = 0.5$. References [28–30] discuss spin 1/2 fermions in the unitary limit based on separable interactions derived from inverse scattering. A review of neutron matter in the low-density regime can be found in Ref. [31].

After a brief review of the theoretical framework (Sec. II), I discuss low-density neutron matter and its behavior at the unitary limit, Sec. III. In Sec. III A, special attention is given to the unitary limit as a constraint for the symmetry energy at normal density. Closely related to the nature of low-density NM as a highly interacting system of fermions is S-wave superfluidity. In Sec. IV, I present baseline results for the singlet gap in NM obtained via the BCS equation. Conclusions, work in progress, and future prospects are found in Sec. V.

II. THEORETICAL FRAMEWORK

The EoS for neutron matter is obtained at the leading-order in the hole-line expansion—namely, via a nonperturbative summation of the particle-particle ladders. The single-neutron potentials are computed self-consistently with the G matrix, employing a continuous spectrum.

The interactions used here are derived from chiral effective field theory (EFT) [3], which provides a path to a consistent development of nuclear forces. Symmetries relevant to low-energy QCD are incorporated in the theory, in particular chiral symmetry. Thus, although the degrees of freedom are pions and nucleons instead of quarks and gluons, there exists a solid connection with the fundamental theory of strong interactions through its symmetries and the mechanism of their breaking. Chiral EFT employs a power counting scheme in which the progression of two- and many-nucleon forces is constructed following a well-defined hierarchy. This allows for the inclusion of all three-nucleon forces (3NFs) which appear at a given order, thus eliminating the inconsistencies which are unavoidable when adopting meson-theoretic or phenomenological forces. Finally, it provides a clear method for controlling the truncation error on an order-by-order basis. Next, I give a brief summary of the input two-nucleon forces (2NFs) and 3NFs. Additional information, including the values of the LECs, can be found in Refs. [1,32].

The 2NF applied in this work are from Ref. [33], a family of high-quality potentials from leading order (LO) to fifth order (N^4LO) of chiral EFT, using a nonlocal regulator [1]. The long-range part of these potentials is tightly constrained by the πN low-energy constants (LECs) from the Roy-Steiner analysis of Refs. [34,35]. This analysis is sufficiently accurate to render errors in the πN LECs essentially negligible for the purpose of quantifying the uncertainty. With the choice $\Lambda = 450$ MeV—which is maintained throughout this paper—the potentials are soft according to the Weinberg eigenvalue analysis of Ref. [36] and the perturbative calculations of infinite matter from Ref. [37].

Three-nucleon forces first appear at the third order of the chiral expansion (N^2LO) of the Δ-less theory, which is the one applied in this work. At this order, the 3NF consists of three contributions [38]: the long-range two-pion-exchange (2PE) graph, the medium-range one-pion-exchange (1PE) diagram, and a short-range contact term.

The 3NF at N^3LO has been derived in Refs. [39,40]. The long-range part of the subleading chiral 3NF consists of three topologies: the 2PE topology, which is the longest-range component of the subleading 3NF, the two-pion-one-pion exchange (2P1PE) topology, and the ring topology, generated by a circulating pion which is absorbed and re-emitted from each of the three nucleons.

In infinite matter, these 3NF can be expressed as density-dependent effective two-nucleon interactions as derived in Refs. [41,42]. They are represented in terms of the well-known nonrelativistic two-body nuclear force operators and, therefore, can be conveniently incorporated in the usual NN partial wave formalism and the particle-particle ladder approximation for computing the EoS. The effective density-dependent two-nucleon interactions at N^2LO consist of six one-loop topologies. Three of them are generated from the 2PE graph of the chiral 3NF and depend on the LECs $c_{1,3,4}$, which are already present in the 2PE part of the NN interaction. Two one-loop diagrams are generated from the 1PE diagram, and depend on the low-energy constant c_D. Finally, there is the one-loop diagram that involves the 3NF contact diagram, with LEC c_E. The last two sets do not contribute in neutron matter.

The in-medium NN potentials corresponding to the long-range subleading 3NFs are given in Ref. [43] for SNM and in Ref. [44] for NM. The short-range subleading 3NF consists of: the one-pion-exchange-contact topology (1P-contact), which gives no net contribution, the two-pion-exchange-contact topology (2P-contact), and relativistic corrections, which depend on the C_S and the C_T LECs of the 2NF and are proportional to $1/M$, where M is the nucleon mass. Expressions for the in-medium NN potentials corresponding to the short-range subleading 3NFs can be found in Ref. [45] for NM.

Before closing this section, it is appropriate to comment on the uncertainty in the energy per neutron in NM due to

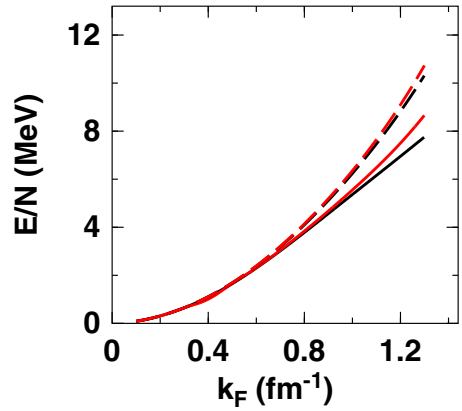

FIG. 1. Energy per neutron in NM vs the Fermi momentum. For either color (black pair or red pair), the solid curve is obtained with all partial waves (up to $J = 15$), while the dashed curve includes only the spin-singlet S wave. The black curves show the result of including only the 2NF, while the red curves are obtained with the inclusion of the full 3NF at N^{3}LO.

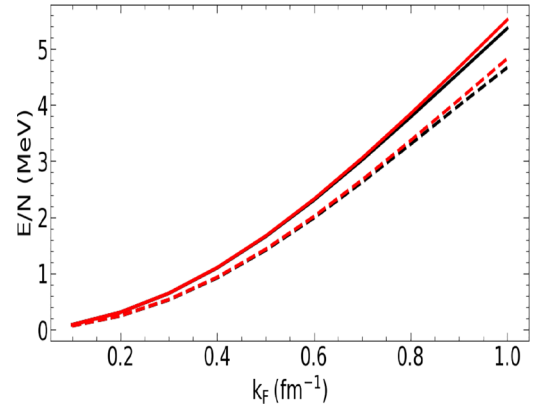

FIG. 2. Black curves: energy per neutron vs the Fermi momentum using the N^{3}LO(450) potential from Ref. [33] (solid) or its nearly unitary counterpart (dashed). Red curves: same comparison with CD-Bonn (solid) and its nearly-unitary version (dashed). The predictions are obtained with the $^1S_0$ channel and the 2NF only.

the use of different many-body theories. In Ref. [37], the authors present a novel Monte Carlo framework for perturbative calculations of both neutron matter and symmetric nuclear matter. Comparing with those predictions (for the same potential from Ref. [33]), we conclude that our results, based on the particle-particle nonperturbative ladder resummation, agree with Ref. [37] within chiral uncertainties. Studies of dependence of the energy per neutron in NM can be found in Refs. [46,47], where three different many-body methods are used with families of coordinate-space potentials.

III. LOW-DENSITY NEUTRON MATTER AND THE UNITARY LIMIT

Here, I discuss some of the remarkable features of low-density NM. I begin with identifying the region of ^{1}S$_0$ dominance, see Fig. 1. The largest (neutron) Fermi momentum included in the figure, 1.3 fm^{-1}, corresponds to a density of 0.074 fm^{-3}, close to one-half of normal nuclear density (taken equal to 0.16 fm^{-3}). One may conclude that the ^{1}S$_0$ channel is dominant up to about $k_F = 1.0$ fm^{-1}. Furthermore, comparing either black curve with the red of corresponding pattern, we see that the impact of the 3NF at these densities is negligible or minor.

The question addressed next is to which extent NM approaches a unitary gas and how its behavior changes if the scattering length tends to (negative) infinity. For this analysis, the Fermi momentum is restricted to values up to 1.0 fm^{-1} and the focus is on the ^{1}S$_0$ channel.

Starting from the chiral potential at N^{3}LO from Ref. [33] with cutoff equal to 450 MeV, I constructed an *ad hoc* potential that is unitary in ^{1}S$_0$, having a scattering length of nearly -10^4 fm—essentially infinity. This comparison is shown in Fig. 2, where the pair of black curves, solid and dashed, are the predictions obtained with the N^{3}LO potential and its unitary version, respectively. I also consider one of the popular high-precision meson-exchange potentials of the 1990s, the CD-Bonn potential [48], and constructed a nearly unitary version for CD-Bonn as well. These are also shown in Fig. 2 as the pair of red curves. In all cases, only the 2NF is included. Although N^{3}LO and CD-Bonn are based on very different philosophies, accurate reproduction of low-energy free-space data is a stringent constraint for neutron matter [2], hence the strong similarity between the two solid (or the two dashed) curves. We also note that the solid and the dashed curves (of either color) differ by less than 1 MeV, consistent with neutron matter approaching the behavior of a unitary system at these densities. It should be emphasized that a change of only a few percent of the leading order contact parameter in ^{1}S$_0$ is sufficient to cause very large variations in a_s, a sensitivity similar to the one seen when tuning of the interaction with magnetic fields in experiments with cold atoms.

In a discussion of unitary gases, it is insightful to display the ratio of the energy of the interacting gas to the energy of a free Fermi gas at the same density—the aforementioned Bertsch parameter. Figure 3 shows such ratio calculated with the original N^{3}LO potential (solid black) and its unitary version (dashed black). An analogous description applies to the pair of red curves, but for CD-Bonn. The two potentials are impacted in almost exactly the same way by enforcing unitarity in $^1S_0$. The nearly unitary interactions show a clear tendency to join the cold atoms results [49], solid squares, towards the unitary limit (where the Bertsch parameter is defined).

Unitarity as a constraint for neutron matter and the symmetry energy

A few years ago, Tews *et al.* [50] proposed the existence of a lower limit on the energy of NM based on unitarity. With an eye on recent results from electroweak scattering, I wish to revisit that discussion for the purpose of emphasising the importance of low-energy constraints for NM and the symmetry energy.

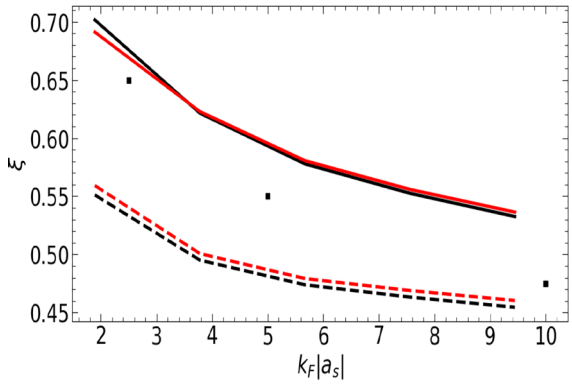

FIG. 3. Energy per neutron in units of the free Fermi energy, ξ. The solid and dashed black curves are obtained with the original N^{3}LO potential and its unitary counterpart, respectively. The same comparison with the CD-Bonn potential and its unitary counterpart is shown by the red solid and dashed curves. The horizontal scale displays the dimensionless parameter $|a_s k_F|$. The filled squares are results from cold atoms [49]. The predictions are obtained with the $^1S_0$ channel and the 2NF only.

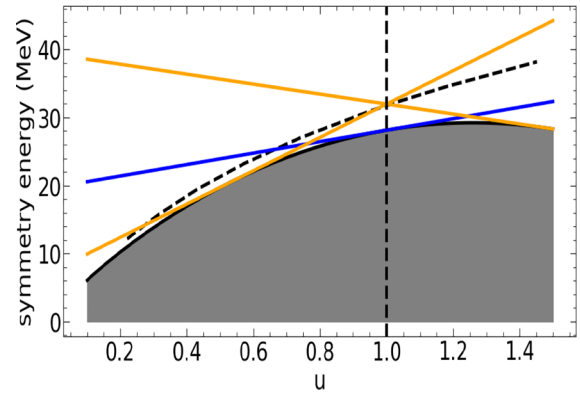

FIG. 4. Lower bound for the symmetry energy from Eq. (8). The grey area is the excluded region for the symmetry energy. The black dashed vertical line marks the saturation density. The blue line is tangent to the lower-bound curve at $u = 1$. As an example, a symmetry energy equal to 32 MeV is chosen. Each of the two yellow lines goes through the chosen value and is tangent to the lower-bound curve at a point with $u < 1$ or $u > 1$. The black short-dashed curve shows the predictions from Ref. [1].

First, note that the predictions in Figs. 2 and 3 are consistent with

$$E_{NM}(\rho) \geqslant E_{UG}(\rho), \tag{3}$$

where UG stands for unitary gas. If this is a general bound—as it seems likely, since higher total energy (that is, less attraction) can be expected in NM as compared to the system with infinitely large neutron-neutron scattering length—then one can write

$$E_{NM}(\rho) \geqslant E_{UG}(\rho) = \xi_0 E_{FG}(\rho), \tag{4}$$

where ξ_0 is the Bertsch parameter, and E_{FG} is the energy of the noninteracting Fermi gas,

$$E_{FG} = \frac{3\hbar^2 k_F^2}{10m}, \quad k_F = (3\pi^2\rho)^{1/3}. \tag{5}$$

Thus, in the parabolic approximation to the symmetry energy, we can write

$$E_{\rm sym}(\rho) = E_{NM}(\rho) - E_{SNM}(\rho) \geqslant E_{UG}(\rho) - E_{SNM}(\rho), \tag{6}$$

where SNM signifies symmetric nuclear matter.

There exist "established" expansions of the energy in SNM in terms of the saturation parameters $E_0 = E(\rho_0)$ and the incompressibility K_0. The next term in the expansion is the skewness, Q_0, which is poorly known. To streamline the notation, we express density in units of saturation density and define $u = \frac{\rho}{\rho_0}$. The expansion of the SNM energy is then written as

$$E_{SNM}(u) = E_{SNM}(u=1) + \frac{K_0}{18}(u-1)^2 + \frac{Q_0}{162}(u-1)^3 + \cdots, \tag{7}$$

where $u = 1$ at $\rho = \rho_0 = 0.16$ fm^{-3}, $E_{SNM}(u=1) = E_0 = -16$ MeV, and $K_0 = 230$ MeV. In Ref. [50], some estimates are made for Q_0. Clearly, reliable constraints on these parameters must be available from independent sources. It must be emphasized, though, that the specific values are not very relevant for the present discussion, which is a qualitative demonstration of how the unitarity constraint propagates.

From Eqs. (6) and (7), ignoring higher-order terms in the SNM expansion, one can write

$$E_{\rm sym}(u) \geqslant E_{UG}(u) - \left(E_0 + \frac{K_0}{18}(u-1)^2 + \frac{Q_0}{162}(u-1)^3\right). \tag{8}$$

Equation (8) sets a lower bound for the symmetry energy, as shown in Fig. 4, where the shaded area is excluded. Furthermore, replacing the symmetry energy with its well-known expansion about saturation density,

$$E_{\rm sym}(u) = E_{\rm sym,0} + \frac{L}{3}(u-1) + \frac{K_{\rm sym}}{18}(u-1)^2 + \cdots,$$
$$E_{\rm sym,0} = E_{\rm sym}(u=1), \tag{9}$$

one can turn Eq. (8) into a constraint for L, the slope of the symmetry energy at saturation. For the purpose of this semianalytical exercise [50], and for consistency, one term beyond the leading order is retained in both the expansion of the symmetry energy and the SNM energy, that is, $Q_0 = K_{\rm sym} = 0$. Thus,

$$E_{\rm sym}(u) \approx E_{\rm sym,0} + \frac{L}{3}(u-1), \tag{10}$$

and Eq. (8) is written as

$$E_{\rm sym,0} + \frac{L}{3}(u-1) \geqslant E_{UG}(u) - \left(E_0 - \frac{K_0}{18}(u-1)^2\right). \tag{11}$$

So, for a chosen value of $E_{\rm sym,0}$, one can write, for $u > 1$,

$$L \geqslant \frac{3}{(u-1)}\left(E_{UG}(u) - E_0 - \frac{K_0}{18}(u-1)^2 - E_{\rm sym,0}\right), \tag{12}$$

and, for $u < 1$,

$$L \leqslant \frac{3}{(u-1)}\left(E_{UG}(u) - E_0 + \frac{K_0}{18}(u-1)^2 - E_{\rm sym,0}\right), \quad (13)$$

thus setting a lower and an upper limit to L. This is shown in Fig. 4 by the two yellow lines passing through the chosen value of $E_{\rm sym,0}$ and tangent to the lower-bound contour at two points, one with $u < 1$ and the other with $u > 1$. For this simple example, the resulting constraint is

$$-18.7\ {\rm MeV} \leqslant L \leqslant 70.5\ {\rm MeV}, \quad (14)$$

where the negative lower limit is a consequence of the approximations we have applied. Proceeding along these lines, one can then construct a contour in the $(L - E_{\rm sym,0})$ plane. Obviously, unitarity is one of many constraints, from both microscopic theory and experiments, to be considered carefully and vetted for consistency. The focal point of this discussion is to emphasize the inherent connection between NM and low-energy few-nucleon systems, due to the proximity of few-nucleon systems to the unitary limit. Some interesting facts can be found in Ref. [51], where correlations were identified between NM and few-nucleon observables. The impact of the isovector component of the free-space 2NF was also emphasized in Ref. [2], where a minor deterioration of the isospin-1 S and P waves was shown to result in an increase by a factor of 1.75 in the NM pressure at normal density.

These discussions are especially timely in view of the recent measurement of the neutron skin in ^{208}Pb from electroweak scattering being in contrast with most microscopic predictions and other measurements [52]. Moreover, the result for the neutron skin in ^{48}Ca from the parity-violating experiment CREX [53] would not be expected based on the PREX-II result.

IV. THE SUPERFLUID SINGLET GAP: BASELINE RESULTS

In this section, the focus moves to the superfluid gap in the singlet channel. A pairing gap is a two-body correlation around the Fermi surface which can manifest itself in any quantum system of fermions. Similar to the formation of Cooper pairs [54] in the presence of the attractive phonon-mediated interaction between electrons, pairing in nuclei leads to the formation of a superfluid state that opens a gap at the Fermi surface and reduces the available phase space. Isovector pairing in NM is relevant for the physics of neutron-rich nuclei, especially halo nuclei, and neutron star matter.

To calculate the gap at the simplest level, it is customary to use the BCS (from the theory of electron superconductivity, now referred to as BCS theory [54]) approximation with the bare two-body potential and free-space single-particle (sp) energies. The gap equation then reads, for an uncoupled state,

$$\Delta(k) = -\frac{1}{\pi}\int_0^\infty \frac{k'^2 V(k,k')\Delta(k')dk'}{\sqrt{(e(k') - e_F)^2 + \Delta^2(k')}}, \quad (15)$$

where $e(k)$ is the single-particle energy, e_F is the Fermi energy, $V(k,k')$ is the pairing interaction, and $\Delta(k)$ the unknown gap function, to be determined in a self-consistent way. Note that the Fermi energy approximates the chemical potential, which should be evaluated self-consistently with the gap. I follow the solution method from Ref. [55], the main steps of which are summarized below.

Following the Khodel's method [55], the potential $V(k,k')$ is decomposed as

$$V(k,k') = V_F\phi(k)\phi(k') + W(k,k'), \quad (16)$$

where $V_F = V(k_F,k_F) \neq 0$ and $\phi(k) = V(k,k_F)/V_F$. Note that $\phi(k_F) = 1$ and $W(k_F,k) = 0$. Employing these definitions and defining a dimensionless gap function through $\Delta(k) = \Delta_F\chi(k)$, Eq. (15) can be written as two equations:

$$\chi(k) = \phi(k) - \frac{1}{\pi}\int_0^\infty \frac{k'^2 W(k,k')\chi(k')dk'}{\sqrt{(e(k') - e_F)^2 + \Delta_F^2\chi^2(k')}} \quad (17)$$

and

$$-\frac{1}{\pi}V_F\int_0^\infty \frac{k'^2\phi(k')\chi(k')dk'}{\sqrt{(e(k') - e_F)^2 + \Delta_F^2\chi^2(k')}} = 1. \quad (18)$$

The advantage of this transformation is that the integrand in Eq. (17) vanishes for $k = k_F$ and thus the nearly singular behavior of the original equation is removed. The solution scheme [55] consists of the following steps: replace $\Delta_F^2\chi^2(k')$ in the denominator of Eq. (17) by some initial (constant) value, say Δ_0, and solve the resulting (now linear) integral equation with standard matrix inversion techniques to obtain a first approximation for $\chi(k)$, say $\chi^{(1)}(k)$; replace $\chi^{(1)}(k)$ into Eq. (18) to obtain a corresponding solution for Δ_F, $\Delta_F^{(1)}$; repeat the iteration scheme until satisfactory convergence is reached. Equation (18) is perhaps more insightful if written as

$$\frac{1}{V_F} + \frac{1}{\pi}\int_0^\infty \phi(k)\frac{k^2(\phi(k) - \chi(k))dk}{\sqrt{(e(k) - e_F)^2 + \Delta_F^2\chi^2(k)}} - \frac{1}{\pi}\int_0^\infty \frac{k^2\phi^2(k)dk}{\sqrt{(e(k) - e_F)^2 + \Delta_F^2\chi^2(k)}} = 0. \quad (19)$$

Recalling that $\chi(k_F) = \phi(k_F) = 0$ and arguing that a major contribution to the integral comes from momenta near the Fermi surface, the second integral in Eq. (18) is expected to be nearly insensitive to Δ_F, which facilitate the convergence.

In Fig. 5, the singlet gap, calculated as described above, is shown in units of the Fermi energy as a function of $k_F|a_s|$. For the purpose of covering a broad spectrum of (bare) interactions, predictions are given for the chiral potential, the meson-exchange CD-Bonn potential, and a local phenomenological potential of the past [56]. While the first two cases are very close, the older local potential generates noticeably lower values of the gap, which can be understood in terms of the weaker attraction typical of local interactions. The dots are from quantum Monte Carlo (QMC) calculations of cold atoms [57]. Neutron matter displays universal behavior up to values

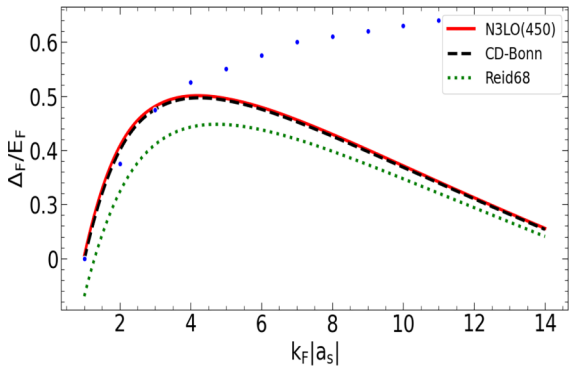

FIG. 5. The singlet gap in units of the Fermi energy obtained with: the chiral interaction (solid red lines), the meson-exchange CD-Bonn potential (black dashed lines), the local phenomenological Reid potential (dotted green lines). Only the 2NF is included. The blue dots are results from QMC calculations of cold atoms.

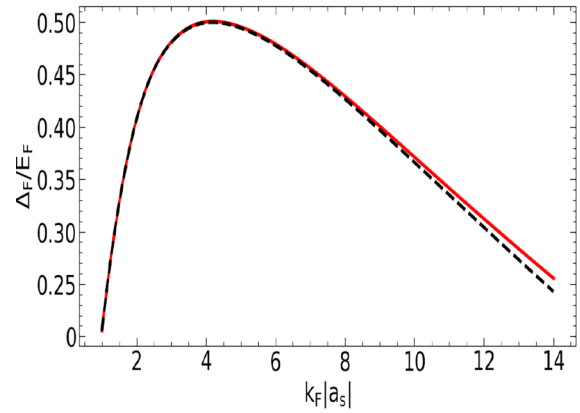

FIG. 6. The singlet gap in units of the Fermi energy. Solid red lines: BCS predictions by the N^{3}LO(450) 2NF. Dashed black lines: 2NF plus 3NF up to N^{3}LO.

of $k_F|a_s|$ approximately equal to 4, at which point it departs from the unitary gas, indicating that finite-range effects are no longer negligible.

Inclusion of 3NFs and other medium effects results in considerable, sometimes extreme, model dependence [57–60]. In Fig. 6, the basic BCS predictions with N^{3}LO(450) are compared with those where both the leading and subleading 3NF are included. At the low densities considered in the figure (up to 9% of saturation density), the effect is a mild reduction.

V. CONCLUSIONS, WORK IN PROGRESS, AND FUTURE PLANS

Dilute NM displays interesting features due to its similarity to a unitary Fermi gas. To explore those features in more depth, nucleon-nucleon potentials with nearly infinite $^1S_0$ neutron-neutron scattering length were constructed. It is important to emphasize that a small tuning of the leading order contact parameter in $^1S_0$ can produce huge variations in the singlet scattering length. The Bertsch parameter is shown and compared with other predictions obtained with ultracold atomic gases.

I discussed the unitarity regime as a significant constraint to normal density neutron matter, the symmetry energy, and its density dependence. I then took the opportunity to underline the importance of a realistic description of low-energy few-nucleon systems for robust predictions of neutron and neutron-rich matter.

A discussion of the singlet pairing gap followed, where I presented baseline results, on which to build systematic calculations including other medium effects besides 3NFs, such as self-consistently determined single-particle energies.

Generally, calculations beyond BCS show a considerable spread of predicted values, depending on which and how medium modifications are included. For the gap in the triplet channel, the status is much more unsettled. For example, in Ref. [61], using two parametrizations of the UIX 3NF the authors find conflicting answers to whether a triplet P-wave gap even exists.

In the inner crust of neutron stars, neutron-rich nuclei are arranged in a crystal lattice surrounded by neutrons in a superfluid state. At densities up to one-half of saturation density, these unbound neutrons form Cooper pairs in the dominant $^1S_0$ state, strongly attractive at low momenta. The physics of the inner crust is largely dependent on this S-wave neutron superfluid, which has been observed through pulsar glitches and modifications of the neutron star cooling due to strong modifications in neutrino emission. I am currently working on systematic predictions of the neutron-neutron pairing gap in the S- and P-wave channels, to be followed by neutron star cooling simulations.

ACKNOWLEDGMENTS

This work was supported by the U.S. Department of Energy, Office of Science, Office of Basic Energy Sciences, under Award No. DE-FG02-03ER41270. I am grateful to A. Gezerlis and G. Palkanoglou for helpful discussions on the pairing gap and the BCS equation.

[1] F. Sammarruca and R. Millerson, Analysis of the neutron matter equation of state and the symmetry energy up to fourth order of chiral effective field theory, Phys. Rev. C **104**, 034308 (2021).

[2] F. Sammarruca, The symmetry energy: Current status of *ab initio* predictions vs. empirical constraints, Symmetry **15**, 450 (2023).

[3] S. Weinberg, Three-body interactions among nucleons and pions, Phys. Lett. B **295**, 114 (1992).

[4] Q. Chen, C. R. Howell, T. S. Carman, W. R. Gibbs, B. F. Gibson, A. Hussein *et al.*, Measurement of the neutron-neutron scattering length using the $\pi - d$ capture reaction, Phys. Rev. C **77**, 054002 (2008).

[5] G. A. Miller, B. M. K. Nefkens, and I. Šlaus, Charge symmetry, quarks and mesons, Phys. Rep. **194**, 1 (1990).

[6] G. A. Baker, Jr., Neutron matter model, Phys. Rev. C **60**, 054311 (1999).

[7] J. Kinast, A. Turlapov, J. E. Thomas, Q. Chen, J. Stajic, and K. Levin, Heat capacity of a strongly-interacting Fermi gas, Science **307**, 1296 (2005).

[8] T. Bourdel, L. Khaykovich, J. Cubizolles, J. Zhang, F. Chevy, M. Teichmann *et al.*, Experimental study of the BEC-BCS crossover region in lithium 6, Phys. Rev. Lett. **93**, 050401 (2004).

[9] G. B. Partridge, W. Li, R. I. Kamar, Y. A. Liao, and R. G. Hulet, Pairing and phase separation in a polarized Fermi gas, Science **311**, 503 (2006).

[10] J. T. Stewart, J. P. Gaebler, C. A. Regal, and D. S. Jin, Potential energy of a 40 K Fermi gas in the BCS-BEC crossover, Phys. Rev. Lett. **97**, 220406 (2006).

[11] L. Luo and J. E. Thomas, Thermodynamic measurements in a strongly interacting Fermi gas, J. Low Temp. Phys. **154**, 1 (2009).

[12] M. J. H. Ku, A. T. Sommer, L. W. Cheuk, and M. W. Zwierlein, Revealing the superfluid lambda transition in the universal thermodynamics of a unitary Fermi gas, Science **335**, 563 (2012).

[13] C. Chin, R. Grimm, P. Julienne, and E. Tiesinga, Feshbach resonances in ultracold gases, Rev. Mod. Phys. **82**, 1225 (2010).

[14] I. Bloch, J. Dalibard, and W. Zwerger, Many-body physics with ultracold gases, Rev. Mod. Phys. **80**, 885 (2008).

[15] S. Giorgini, L. P. Pitaevski, and S. Stringari, Theory of ultracold atomic Fermi gases, Rev. Mod. Phys. **80**, 1215 (2008).

[16] G. Calvanese Strinati, P. Pieri, G. Röpke, P. Schuck, and M. Urban, The BCSBEC crossover: from ultra-cold Fermi gases to nuclear systems, Phys. Rep. **738**, 1 (2018).

[17] H. Heiselberg, Fermi systems with long scattering lengths, Phys. Rev. A **63**, 043606 (2001).

[18] G. M. Bruun, Universality of a two-component Fermi gas with a resonant interaction, Phys. Rev. A **70**, 053602 (2004).

[19] A. Perali, P. Pieri, and G. C. Strinati, Quantitative comparison between theoretical predictions and experimental results for the BCS-BEC crossover, Phys. Rev. Lett. **93**, 100404 (2004).

[20] Y. Nishida and D. T. Son, ϵ expansion for a Fermi gas at infinite scattering length, Phys. Rev. Lett. **97**, 050403 (2006).

[21] R. Haussmann, W. Rantner, S. Cerrito, and W. Zwerger, Thermodynamics of the BCS-BEC crossover, Phys. Rev. A **75**, 023610 (2007).

[22] J. W. Chen and E. Nakano, BEC-BCS crossover in the ϵ expansion, Phys. Rev. A **75**, 043620 (2007).

[23] J. Carlson, S. Gandolfi, K. E. Schmidt, and S. Zhang, Auxiliary-field quantum Monte Carlo method for strongly paired fermions, Phys. Rev. A **84**, 061602 (2011).

[24] H. Dong, L.-W. Siu, and T. T. S. Kuo, and R. Machleidt, Unitary potentials and neutron matter at the unitary limit, Phys. Rev. C **81**, 034003 (2010).

[25] B. Friedman and V. R. Pandharipande, Hot and cold, nuclear and neutron matter, Nucl. Phys. A **361**, 502 (1981).

[26] J. Carlson, J. Morales, V. R. Pandharipande, and D. G. Ravenhall, Quantum Monte Carlo calculations of neutron matter, Phys. Rev. C **68**, 025802 (2003).

[27] M. Baldo and C. Maieron, Neutron matter at low density and the unitary limit, Phys. Rev. C **77**, 015801 (2008).

[28] H. S. Kohler, Spin 1/2 fermions in the unitary limit. I. arXiv:0705.0944 [nucl-th].

[29] H. S. Kohler, Spin 1/2 fermions in the unitary limit. II. arXiv:0801.1123 [nucl-th].

[30] H. S. Kohler, Spin 1/2 fermions in the unitary limit. III. arXiv:1008.3884 [nucl-th].

[31] I. Vidaña, Low-density neutron matter and the unitary limit, Front. Phys. **9**, 660622 (2021).

[32] F. Sammarruca and R. Millerson, Overview of symmetric nuclear matter properties from chiral interactions up to fourth order of the chiral expansion, Phys. Rev. C **104**, 064312 (2021).

[33] D. R. Entem, R. Machleidt, and Y. Nosyk, High-quality two-nucleon potentials up to fifth order of the chiral expansion, Phys. Rev. C **96**, 024004 (2017).

[34] M. Hoferichter, J. R. de Elvira, B. Kubis, and U.-G. Meissner, Matching pion-nucleon Roy-Steiner equations to chiral perturbation theory, Phys. Rev. Lett. **115**, 192301 (2015).

[35] M. Hoferichter, J. R. de Elvira, B. Kubis, and U.-G. Meissner, Roy-Steiner-equation analysis of pion-nucleon scattering, Phys. Rep. **625**, 1 (2016).

[36] J. Hoppe, C. Drischler, R. J. Furnstahl, K. Hebeler, and A. Schwenk, Weinberg eigenvalues for chiral nucleon-nucleon interactions, Phys. Rev. C **96**, 054002 (2017).

[37] C. Drischler, K. Hebeler, and A. Schwenk, Chiral interactions up to next-to-next-to-next-to-leading order and nuclear saturation, Phys. Rev. Lett. **122**, 042501 (2019).

[38] E. Epelbaum, A. Nogga, W. Glöckle, H. Kamada, U.-G. Meißner, and H. Witala, Three nucleon forces from chiral effective field theory, Phys. Rev. C **66**, 064001 (2002).

[39] V. Bernard, E. Epelbaum, H. Krebs, and U.-G. Meißner, Subleading contributions to the chiral three-nucleon force: Long-range terms, Phys. Rev. C **77**, 064004 (2008).

[40] V. Bernard, E. Epelbaum, H. Krebs, and U.-G. Meißner, Subleading contributions to the chiral three-nucleon force. II. Short-range terms and relativistic corrections, Phys. Rev. C **84**, 054001 (2011).

[41] J. W. Holt, N. Kaiser, and W. Weise, Chiral three-nucleon interaction and the ^{14}C-dating β decay, Phys. Rev. C **79**, 054331 (2009).

[42] J. W. Holt, N. Kaiser, and W. Weise, Density-dependent effective nucleon-nucleon interaction from chiral three-nucleon forces, Phys. Rev. C **81**, 024002 (2010).

[43] N. Kaiser and B. Singh, Density-dependent *NN* interaction from subleading chiral three-nucleon forces: Long-range terms, Phys. Rev. C **100**, 014002 (2019).

[44] N. Kaiser, Density-dependent nn-potential from subleading chiral three-neutron forces: Long-range terms, arXiv:2010.02739v4 [nucl-th] (2020).

[45] L. Treuer, Density-dependent neutron-neutron interaction from subleading chiral three-neutron forces, arXiv:2009.11104 [nucl-th] (2009).

[46] M. Piarulli, I. Bombaci, D. Logoteta, A. Lovato, and R. B. Wiringa, Benchmark calculations of pure neutron matter with realistic nucleon-nucleon interactions, Phys. Rev. C **101**, 045801 (2020).

[47] A. Lovato, I. Bombaci, D. Logoteta, M. Piarulli, and R. B. Wiringa, Benchmark calculations of infinite neutron matter with realistic two- and three-nucleon potentials, Phys. Rev. C **105**, 055808 (2022).

[48] R. Machleidt, High-precision, charge-dependent Bonn nucleon-nucleon potential, Phys. Rev. C **63**, 024001 (2001).

[49] A. Gezerlis and J. Carlson, Strongly paired fermions: Cold atoms and neutron matter, Phys. Rev. C **77**, 032801 (2008).
[50] I. Tews, J. M. Lattimer, and A. Ohnishi, Kolomeitsev EE. Symmetry parameter constraints from a lower bound on the neutron-matter energy, Astrophys. J. **848**, 105 (2017).
[51] A. Kievsky, M. Viviani, D. Logoteta, I. Bombaci, and L. Girlanda, Correlations imposed by the unitary limit between few-nucleon systems, nuclear matter, and neutron stars, Phys. Rev. Lett. **121**, 072701 (2018).
[52] B. T. Reed, F. J. Fattoyev, C. J. Horowitz, and J. Piekarewicz, Implications of PREX-II on the equation of state of neutron-rich matter, Phys. Rev. Lett. **126**, 172503 (2021).
[53] D. Adhikari *et al.* (CREX Collaboration), Precision determination of the neutral weak form factor of ^{48}Ca, Phys. Rev. Lett. **129**, 042501 (2022).
[54] J. Bardeen, L. N. Cooper, and J. R. Schrieffer, Theory of superconductivity, Phys. Rev. **108**, 1175 (1957).
[55] V. A. Khodel, V. V. Khodel, and J. W. Clark, Solution of the gap equation in neutron matter, Nucl. Phys. A **598**, 390 (1996).
[56] R. V. Reid, Jr., Local phenomenological nucleon-nucleon potentials, Ann. Phys. **50**, 411 (1968).
[57] S. Gandolfi, G. Palkanoglou, J. Carlson, and A. Gezerlis, The $^1S_0$ pairing gap in neutron matter, Condens. Matter **7**, 19 (2022).
[58] M. Drissi and A. Rios, Many-body approximations to the superfluid gap and critical temperature in pure neutron matter, Eur. Phys. J. A **58**, 90 (2022).
[59] G. E. Pavlou, E. Mavrommatis, Ch. Moustakidis, and J. W. Clark, Microscopic study of $^1S_0$ superfluidity in dilute neutron matter, Eur. Phys. J. A **53**, 96 (2017).
[60] O. Benhar and G. De Rosi, Superfluid gap in neutron matter from a microscopic effective interactions, J. Low Temp. Phys. **189**, 250 (2017).
[61] P. Papakonstantinou and J. W. Clark, Three-nucleon forces and triplet pairing in neutron matter, J. Low Temp. Phys. **189**, 361 (2017).